

First lensing measurements of SZ-detected clusters

Rachel N. McInnes,^{1*} Felipe Menanteau,² Alan F. Heavens,¹ John P. Hughes,²
Raul Jimenez,³ Richard Massey,¹ Patrick Simon¹ and Andy Taylor¹

¹Scottish Universities Physics Alliance (SUPA), Institute for Astronomy, University of Edinburgh, Blackford Hill, Edinburgh EH9 3HJ

²Rutgers University, Department of Physics and Astronomy, 136 Frelinghuysen Road, Piscataway, NJ 08854, USA

³ICREA and ICE(CSIC)–IEEC, UAB campus, Bellaterra 08193, Spain

Accepted 2009 July 28. Received 2009 July 28; in original form 2009 June 14

ABSTRACT

We present the first lensing mass measurements of Sunyaev–Zel’dovich (SZ) selected clusters. Using optical imaging from the Southern Cosmology Survey (SCS), we present weak lensing masses for three clusters selected by their SZ emission in the South Pole Telescope (SPT) survey. We confirm that the SZ selection procedure is successful in detecting mass concentrations. We also study the weak lensing signals from 38 optically-selected clusters in $\simeq 8 \text{ deg}^2$ of the SCS survey. We fit Navarro, Frenk and White (NFW) profiles and find that the SZ clusters have amongst the largest masses, as high as $5 \times 10^{14} M_{\odot}$. Using the best-fitting masses for all the clusters, we analytically calculate the expected SZ integrated Y parameter, which we find to be consistent with the SPT observations.

Key words: gravitational lensing – galaxies: clusters: general – cosmology: observations.

1 INTRODUCTION

Galaxy clusters are the largest gravitationally bound objects in the Universe and can be used as cosmological probes because their formation and evolution rate are sensitive to different cosmological parameters (e.g. Evrard 1989; Haiman, Mohr & Holder 2001; Allen et al. 2004). The abundance of galaxy clusters as a function of mass $N(m, z)$ at high redshift z is particularly sensitive to different cosmological models. To probe cosmology and dark energy, we must observe galaxy clusters at high redshift and obtain mass estimates for them.

Observations of the Sunyaev–Zel’dovich (SZ) effect (Sunyaev & Zel’dovich 1981) are a powerful way to probe galaxy clusters by detecting the hot cluster gas (Birkinshaw 1999). SZ-detected clusters are in principle particularly powerful as they can be seen to high redshifts. The intensity of the SZ effect summed over the entire cluster closely tracks the mass of the cluster (Motl, Hallman & Burns 2005). X-ray or SZ effect mass estimates are based on simplified assumptions such as a hydrostatic equilibrium for the cluster gas. It is becoming increasingly apparent, however, that we cannot fully model the complex gas physics in clusters within a simple framework. Nonetheless, it will be very challenging to calibrate cluster masses at high redshift, so in order to use SZ observations to probe cluster properties and cosmological models it is important to understand the relationship between mass and SZ observables in lower redshift systems. Gravitational lensing facilitates the calibration of the SZ observables to obtain accurate masses for SZ detections (Lewis & King 2006; Sealfon, Verde &

Jimenez 2006). A large area in the southern sky is currently being surveyed in SZ by the Atacama Cosmology Telescope (ACT) and the South Pole Telescope (SPT).

Gravitational lensing is dependent only on the projected mass distribution of the lens, and so it is possible to study the mass distribution independent of its form, including the distribution of dark matter. Gravitational lensing causes small (\sim a few per cent) changes to the shape of individual galaxies, which can be used to reconstruct the mass distribution in the region (Kaiser & Squires 1993); for a review see Munshi et al. (2008). In this Letter, we present measurements of weak lensing masses for clusters which were, for the first time, detected blind by their SZ decrement (Staniszewski et al. 2009). We also include mass measurements from 24 optically detected clusters. This Letter is structured as follows: in Section 2, we present the data and discuss the image processing; Section 3 describes the gravitational lensing methods used; the mass measurements are presented in Section 4 and we compare with measurements from other techniques and calculate the Y parameters. Throughout this Letter, we assume a flat cosmology with $\Omega_m = 0.27$, $\Omega_{\Lambda} = 0.73$ and $H_0 = 100 h \text{ km s}^{-1} \text{ Mpc}^{-1}$ with $h = 0.71$.

2 OBSERVATIONS

We use publicly available data from the Blanco Cosmology Survey – a National Optical Astronomy Observatory Large Survey Project observing 60 nights over 4 years on the Blanco 4 m telescope at the Cerro Tololo InterAmerican Observatory in Chile. The Mosaic II camera is being used for a deep, four-band optical (*griz*) survey of two 50 deg^2 patches of the southern sky. Two areas of southern sky have been targeted, centred on $23^{\text{h}}00^{\text{m}}$, $-55^{\circ}12^{\text{m}}$ and $05^{\text{h}}30^{\text{m}}$, $-52^{\circ}47^{\text{m}}$. These fields lie within a larger area of the

*E-mail: rmm@roe.ac.uk

southern sky which ACT and SPT plan to survey. The Letter is based on observations taken in 2005, with the exception of two clusters from 2006 data. The seeing varies between 0.81 and 1.09 arcsec with a mean of 0.89 arcsec. The image reduction was carried out using the Rutgers Southern Cosmology Pipeline (flat-field correction, CCD calibration, removal of saturated star-bleed trails and bad pixel masks). Next the images were aligned, stacked and median combined using SWARP (Bertin 2006); an astrometric solution was found by matching stars to sources in the US Naval Observatory Catalog. Additional masks were made to remove saturated stars, satellite trails and other blemishes in the image, removing 8 per cent in total. For more information, see Menanteau et al. (2009). Note that we use AB magnitudes throughout. To calculate photometric redshifts (photo- z s), multiband SExtractor (Bertin & Arnouts 1996) g, r, i, z isophotal magnitudes were used to find redshift probability distributions of each object. This was done using the BPZ code (Benítez 2000); see also Menanteau et al. (2009). We focused on four clusters found in SZ (Staniszewski et al. 2009) and also 38 optical clusters selected from $\simeq 8 \text{ deg}^2$ (Menanteau et al. 2009). Of the 38 clusters, we found non-zero mass estimates for 24 clusters, and upper limits for the remaining clusters. We do not consider five of the clusters as they are in regions only observed in a single exposure.

3 WEAK LENSING ANALYSIS

We used the i -band data, three co-added exposures of 450s each, for our shear analysis, and measured galaxy shapes using the Kaiser, Squires & Broadhurst (1995) (KSB) method. Our pipeline is based on Bacon, Refregier & Ellis (2000) and labelled ‘MB’ in Heymans et al. (2006), but has been automated to process rapidly the large Southern Cosmology Survey (SCS) data set. The method deviates from ‘MB’ in automated star/galaxy separation and in point spread function (PSF) interpolation. We tested the pipeline against simulated images from the Shear TEsting Programme (STEP) (see Heymans et al. 2006; Massey et al. 2007). Our method underestimates shear, but consistently throughout a wide range of observing conditions, which is henceforth compensated for in our shear measurements by applying a calibration factor of $1/(0.82 \pm 0.05)$, similar to ‘MB’.

As in ‘MB’ our pipeline locates galaxies via the IMCAT¹ HFINDPEAKS algorithm and measures their quadrupole shape moments using a Gaussian weight function of width $4r_g$, where r_g is the size of the best-fitting Gaussian. The pipeline fits the shear polarizability factor $\frac{1}{2}\text{Tr}(P^\nu)$ as a function of galaxy size. We excluded galaxies smaller than 1.1 times the measured seeing, and those with signal-to-noise ratio (S/N) < 5 , leaving 9 arcmin⁻² to $i \sim 23$. The median redshift is 0.65 (Coil et al. 2004); 69 per cent of galaxies in our catalogue also had photo- z s, which have a consistent z distribution (Menanteau et al. 2009). Departing from the ‘MB’ pipeline, we performed star/galaxy separation via the automated THELI algorithm (Erben et al. 2005), and automated the removal of galaxies with abnormally large values of shear polarizability, smear polarizability or ellipticity, which was present in the ‘MB’ method but labour intensive and slow. The observed shapes of galaxies were finally corrected for the blurring effect of the PSF. We measured the PSF using the 0.5 unsaturated stars arcmin⁻² with $22.0 > i > 18.1$ S/N 55 to 1670. The PSF ellipticity is 0.035 ± 0.019 , where the error is the standard deviation throughout the survey. Optical effects

and temporal variation of the atmosphere and telescope between dithered exposures produce patterns in PSF size and ellipticity. This variation was fitted as a sum of polynomials (of the order of 4 in the x and y directions) plus sums of sines and cosines (of orders up to 4 in x and 8 in y). These choices give a small rms residual $|e|$ of 0.0092.

We estimate masses by fitting an NFW profile (Navarro, Frenk & White 1996) to the average tangential shear from IMCAT’s ETPROFILE routine. The concentration index of the halo was taken as a function of mass and cluster redshift (Dolag et al. 2004). For a robust treatment of missing regions of data, we use a Wiener-filtered mass reconstruction method (Hu & Keeton 2002). To address the mass-sheet degeneracy, the average surface mass density is set to zero over the whole field of view (half a square degree). For the SPT clusters, the peaks of the surface mass density in the Wiener-filtered maps were, where present, assumed to be at the centre of the cluster, otherwise (SPT 0547–5345) the luminosity-weighted centre was used. The latter procedure was followed for the optically selected clusters. Our Wiener-filtered reconstruction was done as follows: the two-point correlation function of the lensing convergence, used as prior for the Wiener reconstruction, was estimated from the shear–shear correlation (Bartelmann & Schneider 2001) $\xi_+(\theta)$ in the data itself. In order to have a smooth prior, we fitted the measured ξ_+ with $\xi_+(\theta) = a/(1 + b\theta)$ where a and b are constants determined by the fit. To obtain S/N maps of the lensing maps, we divided the maps by the rms of 500 noise realizations, which were generated by randomly rotating the ellipticities of the sources followed by a Wiener reconstruction. The S/N maps were then used to confirm the cluster centres found in the mass maps.

4 RESULTS

Wiener-filtered mass reconstructions for three of the SPT SZ-detected clusters are shown in Fig. 1. The fourth SZ cluster at redshift $z \sim 0.88$ was not detected. Our mass maps of clusters SPT 0517–5430, SPT 0509–5342 and SPT 0528–5300 have peak S/N = 3.2, 3.0 and 2.5, respectively. The mass reconstruction of SPT 0528–5300, at $z \sim 0.7$, is shown in the lower panel of Fig. 1. There is a second peak (S/N = 3.5) which may warrant further investigation; it is 6.5 arcmin from the brightest cluster galaxy (BCG). It is at $05^{\text{h}}27^{\text{m}}46^{\text{s}}.2, -53^{\text{h}}07^{\text{m}}57^{\text{s}}.9$ and we estimate it to be $8.12^{+5.03}_{-7.34} \times 10^{14} M_\odot$. On examination of Staniszewski et al. (2009, fig. 1), a small decrement in the SZ appears to be present. There is no statistically significant difference between the redshift distribution of galaxies in a 3 arcmin radius around this location compared to the redshift distribution of the surrounding 0.4 deg^2 region.

Fig. 2 shows the average convergence in circular B-mode apertures for the three detected SPT clusters and for the offset peak. In red (empty circles), we show the B-mode which suggests that the shear catalogues are reasonably free of systematics. Fig. 3 compares lensing and optical mass estimates. We see that the SZ-discovered detections are amongst the most massive of the clusters $\geq 3 \times 10^{14} M_\odot$. M_{L200} is an estimate of the mass, calibrated by weak lensing measurements for SDSS clusters (Reyes et al. 2008), within a radius r_{200} in which the number density is estimated to be $200/\Omega_m$ times the average galaxy number density. This is subject to uncertainties in bias, but is claimed to be an unbiased (to 5 per cent) estimate of the radius where the mass density is 200 times the critical density (Johnston et al. 2007). The uncertainty in M_{L200} is estimated to be a factor of 2 (Menanteau et al. 2009) due to the uncertainty in extrapolating the scaling relation to higher redshifts and uncertain cluster membership. The correlation between the optical

¹ <http://www.ifa.hawaii.edu/~kaiser/imcat>

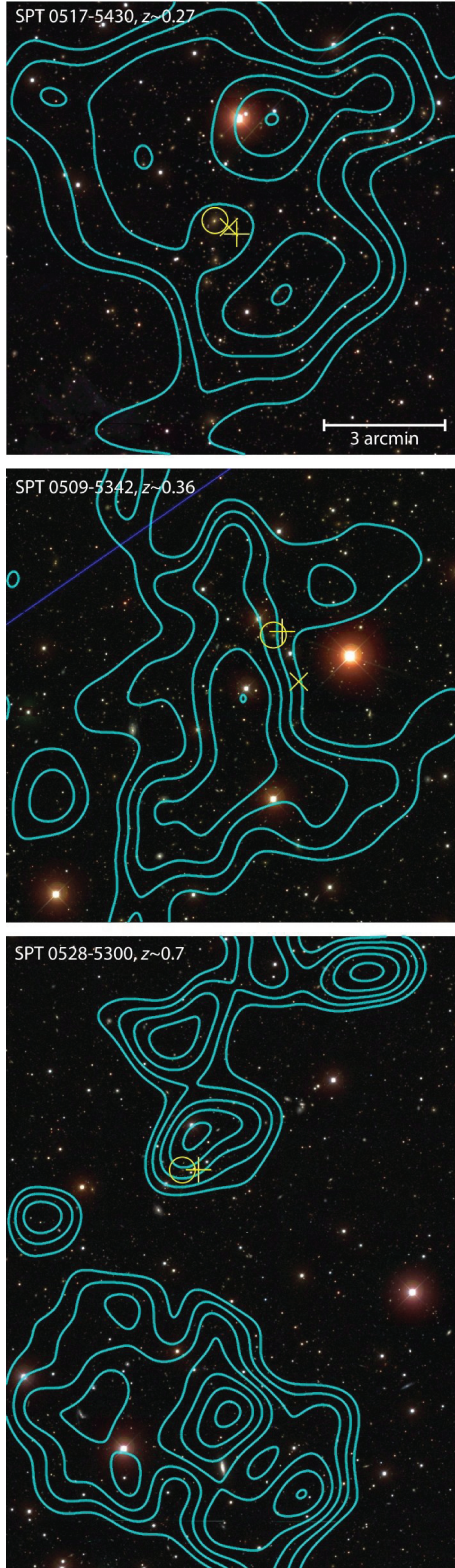


Figure 1. Lensing mass reconstructions for SZ-detected clusters. Contours show the projected lensing convergence (mass distribution), at 1, 1.5, 2, . . . , 4 per cent. A circle indicates the BCG in each optically selected cluster, an \times indicates a peak in X-ray emission and a + denotes the SZ peak.

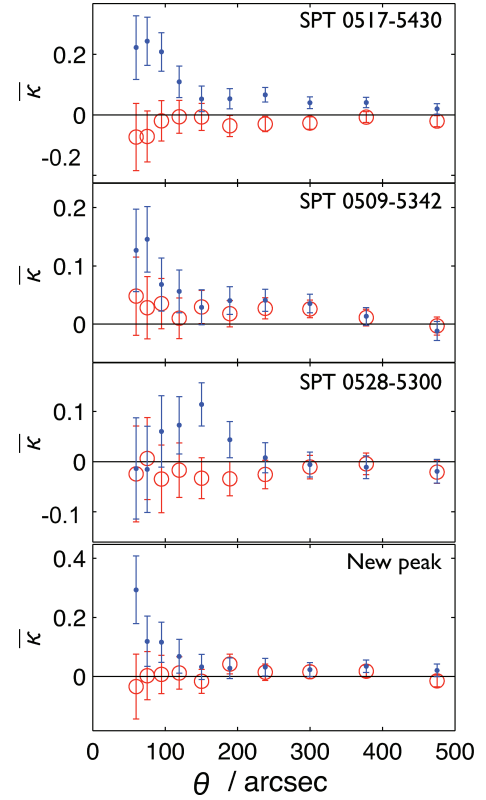


Figure 2. Average convergence within an aperture, $\bar{\kappa}(\theta)$ for the three detected SPT clusters plus the new offset peak found near SPT 0528–5300. The red (empty circle) shows the B-mode systematic error.

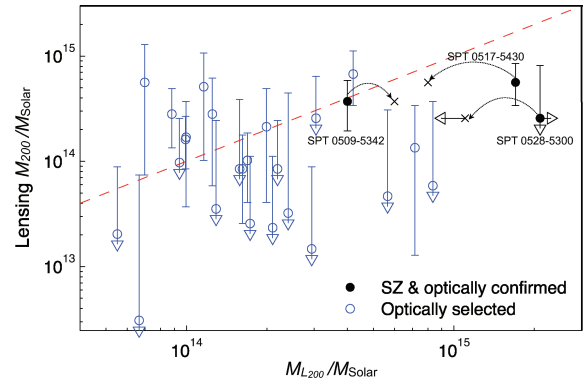


Figure 3. Lensing mass M_{200} measurement against optical mass M_{L200} for SZ and optically selected clusters. Filled circles show the SZ-selected and optically confirmed clusters, while empty circles denote clusters observed optically. Lower error bars marked with a triangle signify that the lower error reaches zero. X-ray mass estimates are shown as an \times in this plot for the three SZ-detected clusters, joined by an arc to the optical estimate. The dashed line is $M_{L200} = M_{200}$ to guide the eye. The uncertainty in M_{L200} is estimated to be a factor 2 (Menanteau et al. 2009).

masses (Menanteau et al. 2009; Menanteau & Hughes 2009) and the weak lensing masses gives some justification for using the optical luminosity as a mass proxy. Interestingly, the most discrepant of the SZ clusters has conflicting optical and X-ray mass estimates, suggesting that M_{L200} is overestimated.

We have also calculated the expected Compton y parameter and its integral over solid angle, $Y \equiv \int d\Omega y(\Omega)$ for the clusters. In Tables 1 and 2, we show the expected temperature decrement in

Table 1. Physical properties of SZ selected clusters in the SCS regions.

ID	RA	Dec.	Centre	z_{photo}	M_{L200}	M_{LX}	M_{200}^{Lens}	$2T_{\text{CMB}} (\text{y})$	Y
		Centre of NFW fit			($10^{14} M_{\odot}$)	($10^{14} M_{\odot}$)	($10^{14} M_{\odot}$)	(μK)	(10^{-5} arcmin 2)
SPT 0517–5430	05:16:27.3	–54:27:39.4	map	$0.27^{+0.02}_{-0.02}$	17	8	$5.61^{+2.88}_{-2.23}$	280^{+150}_{-114}	303^{+170}_{-150}
SPT 0509–5342	05:09:24.4	–53:43:34.4	map	$0.36^{+0.02}_{-0.02}$	4	6	$3.54^{+2.07}_{-1.68}$	219^{+133}_{-106}	129^{+40}_{-40}
SPT 0528–5300	05:28:04.8	–52:58:55.6	map	$0.70^{+0.03}_{-0.02}$	≥ 21	< 11	$2.94^{+5.94}_{-2.94}$	384^{+839}_{-384}	63^{+130}_{-63}
SPT 0547–5345	05:46:41.1	–53:44:52.1	lum.	$0.88^{+0.08}_{-0.04}$	≥ 4	10	–	–	–

Note. Redshifts are the photometric redshift of the BCG, with $\pm 1\sigma$ limits. The ID is based on the position of the BCG. The NFW fit is centred at either the peak in the mass map (map) where available, or the luminosity-weighted centre (lum.). The uncertainty in M_{L200} is estimated to be a factor 2 (Menanteau et al. 2009). Values of $2T_{\text{CMB}} (\text{y})$ and Y are predicted from M_{200}^{Lens} using equation (1). Note that ΔT_{SZ} at 150GHz is 0.29 of the penultimate column value.

Table 2. As Table 1, but for optically selected clusters in the SCS regions. The NFW fit is centred at the luminosity-weighted centre.

ID	RA	Dec.	z_{photo}	M_{L200}	M_{200}^{Lens}	$2T_{\text{CMB}} (\text{y})$	Y
		Centre of NFW fit		($10^{14} M_{\odot}$)	($10^{14} M_{\odot}$)	(μK)	(10^{-5} arcmin 2)
SCSO J232540.2–544430.9	23:25:32.2	–54:44:21.5	0.10 ± 0.02	2.10	$0.23^{+0.89}_{-0.23}$	7^{+88}_{-7}	6^{+75}_{-6}
SCSO J232230.9–541608.3	23:22:27.2	–54:16:26.9	0.12 ± 0.02	1.62	$0.85^{+0.92}_{-0.59}$	27^{+64}_{-23}	39^{+93}_{-33}
SCSO J233000.4–543707.7	N/A		0.14 ± 0.02	1.19	–	–	–
SCSO J232419.6–552548.9	23:24:33.6	–55:26:14.4	0.18 ± 0.04	1.19	< 0.26	–	–
SCSO J233106.9–555119.5	23:31:08.2	–55:50:56.4	0.19 ± 0.04	0.55	$0.20^{+0.69}_{-0.20}$	8^{+83}_{-8}	2^{+19}_{-2}
SCSO J233252.9–561454.1	23:32:51.4	–56:15:29.8	0.20 ± 0.03	1.17	< 0.09	–	–
SCSO J233215.5–544211.6	23:32:17.1	–54:42:43.1	0.20 ± 0.04	1.69	$1.02^{+0.84}_{-0.61}$	40^{+70}_{-32}	25^{+42}_{-19}
SCSO J233037.1–554338.8	23:30:34.8	–55:43:41.5	0.20 ± 0.04	0.99	$1.62^{+1.07}_{-0.77}$	65^{+44}_{-31}	68^{+50}_{-24}
SCSO J233550.6–552820.4	23:35:46.4	–55:29:21.3	0.22 ± 0.04	0.67	$0.03^{+0.71}_{-0.03}$	1^{+250}_{-1}	$0.1^{+21}_{-0.1}$
SCSO J232200.4–544459.7	23:22:01.8	–54:45:38.8	0.27 ± 0.04	1.73	$0.26^{+0.86}_{-0.26}$	12^{+125}_{-12}	2^{+18}_{-2}
SCSO J233522.6–553237.0	23:35:20.0	–55:32:30.9	0.29 ± 0.04	2.19	$0.85^{+1.60}_{-0.85}$	42^{+205}_{-42}	11^{+55}_{-11}
SCSO J233807.5–560304.9	23:38:07.7	–56:02:55.0	0.30 ± 0.04	2.60	< 0.64	–	–
SCSO J232956.0–560808.3	23:29:55.8	–56:08:28.2	0.32 ± 0.04	1.99	$2.13^{+2.75}_{-1.73}$	117^{+350}_{-110}	49^{+75}_{-46}
SCSO J232839.5–551353.8	23:28:41.0	–55:13:25.2	0.32 ± 0.05	1.00	$1.69^{+2.01}_{-1.32}$	92^{+249}_{-85}	33^{+88}_{-30}
SCSO J232633.6–550111.5	23:26:31.1	–55:01:26.9	0.32 ± 0.05	2.81	< 0.48	–	–
SCSO J233753.8–561147.6	23:37:57.1	–56:12:05.8	0.33 ± 0.04	2.94	$0.15^{+0.74}_{-0.15}$	8^{+148}_{-8}	1^{+9}_{-1}
SCSO J232156.4–541428.8	23:21:55.5	–54:14:20.0	0.33 ± 0.04	1.25	< 0.71	–	–
SCSO J233003.6–541426.7	23:30:06.3	–54:13:58.9	0.33 ± 0.04	0.88	$2.81^{+2.07}_{-1.47}$	160^{+241}_{-113}	75^{+114}_{-53}
SCSO J233231.4–540135.8	N/A		0.33 ± 0.04	1.67	–	–	–
SCSO J233430.2–543647.5	N/A		0.35 ± 0.05	3.59	–	–	–
SCSO J233110.6–555213.5	23:31:08.4	–55:51:38.3	0.39 ± 0.05	1.04	< 0.56	–	–
SCSO J233618.3–555440.3	23:32:13.8	–55:54:16.4	0.49 ± 0.03	0.94	$0.97^{+1.59}_{-0.97}$	78^{+314}_{-78}	9^{+36}_{-9}
SCSO J233706.3–541903.8	23:37:11.3	–54:18:57.5	0.51 ± 0.04	1.58	$0.85^{+3.03}_{-0.85}$	71^{+820}_{-71}	7^{+80}_{-7}
SCSO J233816.9–555331.1	23:38:12.7	–55:53:12.5	0.52 ± 0.03	1.29	$0.35^{+2.09}_{-0.35}$	29^{+711}_{-29}	2^{+37}_{-2}
SCSO J233556.8–560602.3	23:35:55.6	–56:05:50.5	0.52 ± 0.03	7.15	$1.35^{+2.03}_{-1.22}$	117^{+423}_{-114}	15^{+54}_{-15}
SCSO J232619.8–552308.8	23:26:14.5	–55:23:22.9	0.52 ± 0.03	1.25	$2.81^{+3.34}_{-2.22}$	250^{+672}_{-231}	52^{+140}_{-48}
SCSO J233425.6–542718.0	23:34:26.9	–54:27:32.5	0.53 ± 0.04	3.41	< 0.37	–	–
SCSO J232215.9–555045.6	23:22:17.0	–55:50:07.1	0.56 ± 0.04	2.40	$0.32^{+4.13}_{-0.32}$	29^{+2303}_{-29}	1^{+103}_{-1}
SCSO J232247.6–541110.1	23:22:53.0	–54:10:54.8	0.58 ± 0.04	1.16	$5.11^{+5.57}_{-4.09}$	532^{+1286}_{-495}	138^{+333}_{-129}
SCSO J232211.0–561847.4	23:22:13.6	–56:18:35.7	0.61 ± 0.05	5.65	$0.47^{+2.61}_{-0.47}$	48^{+1045}_{-48}	2^{+50}_{-2}
SCSO J233731.7–560427.9	23:37:30.0	–56:04:01.2	0.61 ± 0.05	3.05	$2.56^{+3.87}_{-2.56}$	276^{+1005}_{-276}	41^{+149}_{-41}
SCSO J234012.6–541907.2	23:40:08.8	–54:19:02.9	0.62 ± 0.04	5.23	< 2.56	–	–
SCSO J234004.9–544444.8	23:40:02.9	–54:44:21.0	0.66 ± 0.05	4.20	$6.74^{+4.45}_{-3.36}$	843^{+1118}_{-575}	212^{+281}_{-145}
SCSO J232342.3–551915.1	23:23:45.5	–55:19:08.9	0.67 ± 0.04	2.72	< 0.51	–	–
SCSO J232829.7–544255.4	23:28:27.5	–54:42:19.3	0.68 ± 0.04	8.34	$0.59^{+3.12}_{-0.59}$	69^{+1409}_{-69}	3^{+67}_{-3}
SCSO J233403.7–555250.7	N/A		0.71 ± 0.04	0.88	–	–	–
SCSO J233951.1–551331.3	N/A		0.73 ± 0.04	1.3	–	–	–
SCSO J233720.2–562115.1	23:37:22.4	–56:20:44.8	0.75 ± 0.03	0.70	$5.61^{+7.24}_{-4.87}$	835^{+2488}_{-806}	151^{+450}_{-145}

the Rayleigh–Jeans limit $\langle -\Delta T_{RJ} \rangle = 2T_{\text{CMB}} \langle y \rangle$, averaged within r_{200} . At 150 GHz, the actual decrement is smaller by a factor 0.29 (Carlstrom, Holder & Reese 2002, fig. 2). To compute Y , we assume that gas follows dark matter and obtain an analytic result. It ignores the gas history (cf. Reid & Spergel 2006) but our simple model agrees, within 25 per cent, with the empirical scaling relations of Motl et al. (2005) and Nagai (2006), and is supported by Atrio-Barandela et al. (2008) who show from stacked SZ clusters that the baryon profile is consistent with NFW. Y as a function of M_{200} is

$$Y = \frac{\sigma_T}{6\alpha m_e c^2} \left(\frac{\Omega_b}{\Omega_m} \right) \frac{1}{D_A^2} \frac{\delta_{200}^{1/3} M_{200}^{5/3} c_s (1+z) (GH_0)^{2/3}}{[\ln(1+c_s) - c_s/(1+c_s)]^2}, \quad (1)$$

where D_A is the angular diameter distance, M_{200} is the mass within an overdensity $\delta_{200} = 200$ with respect to the mean mass density, α is the total pressure divided by the electron pressure. We assume that ions and electrons are in thermal equilibrium with a Helium mass fraction of 0.24, so $\alpha = 1.93$. We also assume the concentration index

$$c_s(M_{200}) = 9.59(1+z)^{-1} (M_{200}/10^{14} h^{-1} M_\odot)^{-0.102} \quad (2)$$

(Dolag et al. 2004), but note that this is for a $\sigma_8 = 0.9$ cosmology, higher than current estimates (Komatsu et al. 2009). Values of Y were predicted for clusters with mass detections, with statistical errors which are dominated by the error in M_{200}^{Lens} .

With a uniform prior on masses, we record in Table 1 the most likely masses and asymmetric one-sigma errors for the SPT SZ clusters. X-ray masses from soft X-ray luminosity using the correlations in Reiprich & Böhringer (2002) are shown in Table 1. Predicted Y and average y within r_{200} are also shown here, along with the cluster centre used. To the extent that we can estimate $\langle y \rangle$ from the published maps, our results seem to be about 50 per cent higher than observed, but within the errors expected from the mass determinations. Recent ACT SZ measurements (Hincks et al. 2009) are in agreement with our predictions for the two low-redshift clusters which we can compare. Observations of SPT 0517–5430 with *XMM-Newton* yield an X-ray mass within r_{500} of $6.4 \times 10^{14} M_\odot$ (Zhang et al. 2006). Table 2 shows mass measurements and predicted Y and average y within r_{200} for the optically-detected clusters.

5 CONCLUSIONS

There has been longstanding optimism that SZ selection would be among the most favourable ways of detecting clusters for cosmological studies, since simulations show that the SZ detection threshold corresponds very nearly to a threshold in mass. Despite this, it was not guaranteed that the first SZ experiments could trace mass. In order to demonstrate this, we have measured, for the first time, weak lensing masses of clusters detected by their SZ signature. Of the four clusters detected by the SPT and published recently by Staniszewski et al. (2009), we have detected three of them, using optical imaging data from the SCS. The fourth cluster, at redshift of 0.88, is too distant to be detected with these optical data. By fitting NFW profiles, we have established that the published SZ peaks correspond to mass regions, and so we can confirm that the first instalment of SZ selected clusters trace the most massive clusters.

We have also presented weak lensing mass estimates for other clusters detected optically in the SCS. As one might expect, the published SZ clusters have masses at the upper end of the sample

$10^{14} - 10^{15} M_\odot$. Furthermore, we have presented analytic predictions for the integrated Compton Y parameter for all the clusters in the sample for future comparison with SZ observations.

ACKNOWLEDGMENTS

The authors thank Catherine Heymans for many useful discussions. RNM acknowledges the award of an STFC studentship. FM and JPH acknowledge financial support from the National Science Foundation under the PIRE program (award number OISE-0530095). RM acknowledges financial support through FP7 grant MIRG-CT-208994 and STFC Advanced Fellowship PP/E006450/1. We acknowledge the support of the European DUEL Research Training Network (MRTN-CT-2006-036133).

REFERENCES

- Allen S. W., Schmidt R. W., Ebeling H., Fabian A. C., van Speybroeck L., 2004, *MNRAS*, 353, 457
- Atrio-Barandela F., Kashlinsky A., Kocevski D., Ebeling H., 2008, *ApJ*, 675, L57
- Bacon D., Refregier A., Ellis R., 2000, *MNRAS*, 318, 625
- Bartelmann M., Schneider P., 2001, *Phys. Rep.*, 340, 291
- Benítez N., 2000, *ApJ*, 536, 571
- Bertin E., 2006, *SWARP RESAMPLE AND COADD SOFTWARE*. <http://astromatic.iap.fr/software/swarp>
- Bertin E., Arnouts S., 1996, *A&AS*, 117, 393
- Birkinshaw, 1999, *Phys. Rep.*, 310, 97
- Carlstrom J. E., Holder G. P., Reese E. D., 2002, *ARA&A*, 40, 643
- Coil A., Newman J., Kaiser N., Davis M., Ma C., Kocevski D., Koo D., 2004, *ApJ*, 617, 765
- Dolag K., Bartelmann M., Perrotta F., Baccigalupi C., Moscardini L., Meneghetti M., Tormen G., 2004, *A&A*, 416, 853
- Erben T. et al., 2005, *Astronomische Nachrichten*, 326, 432
- Evrard A. E., 1989, *ApJ*, 341, L71
- Haiman Z., Mohr J. J., Holder G. P., 2001, *ApJ*, 553, 545
- Heymans C. et al., 2006, *MNRAS*, 371, 750
- Hincks A. D. et al., 2009, *ApJ*, submitted (arXiv:0907.0461)
- Hu W., Keeton C. R., 2002, *Phys. Rev. D*, 66, 6
- Johnston D. E. et al., 2007, preprint (arXiv:0709.1159)
- Kaiser N., Squires G., 1993, *ApJ*, 404, 441
- Kaiser N., Squires G., Broadhurst T., 1995, *ApJ*, 449, 460
- Komatsu E. et al., 2009, *ApJS*, 180, 330
- Lewis A., King L., 2006, *Phys. Rev. D*, 73, 063006
- Massey R. et al., 2007, *MNRAS*, 376, 13
- Menanteau F., Hughes J. P., 2009, *ApJ*, 694, 136
- Menanteau F. et al., 2009, *ApJ*, 698, 1221
- Motl P. M., Hallman E. J., Burns J. O., 2005, *ApJ*, 623, 63
- Munshi D., Valageas P., van Waerbeke L., Heavens A. F., 2008, *Phys. Rev.*, 462, 67
- Nagai D., 2006, *ApJ*, 650, 538
- Navarro J. F., Frenk C. S., White S. D. M., 1996, *ApJ*, 462, 563
- Reid B. A., Spergel D. N., 2006, *ApJ*, 651, 643
- Reiprich T. H., Böhringer H., 2002, *ApJ*, 567, 716
- Reyes R., Mandelbaum R., Hirata C., Bahcall N., Seljak U., 2008, *MNRAS*, 390, 1157
- Sealfon C., Verde L., Jimenez R., 2006, *ApJ*, 649, 118
- Staniszewski Z. et al., 2009, *ApJ*, 701, 32
- Sunyaev R., Zel'dovich Y., 1981, *Astrophys. Space Phys. Rev.*, 1, 1
- Zhang Y.-Y., Böhringer H., Finoguenov A., Ikebe Y., Matsushita K., Schuecker P., Guzzo L., Collins C. A., 2006, *A&A*, 456, 55

This paper has been typeset from a $\text{\TeX}/\text{\LaTeX}$ file prepared by the author.